Phys Chem Minerals (2003) 30: 1 – 11
DOI 10.1007/s00269-002-0288-9

ORIGINAL PAPER

S. V. Churakov · N. R. Khisina · V. S. Urusov
R. Wirth

First-principles study of $(MgH_2SiO_4)\bullet n(Mg_2SiO_4)$ hydrous olivine structures. I. Crystal structure modelling of hydrous olivine Hy-2*a* $(MgH_2SiO_4) \bullet 3(Mg_2SiO_4)$

Received: 7 February 2002 / Accepted: 23 October 2002

Abstract Recently, the Hy-2*a* hydrous olivine $(MgH_2SiO_4)\cdot 3(Mg_2SiO_4)$ occurring as nanometre-sized inclusions in mantle olivines has been found by TEM, and has been suggested to be a new DHMS phase (Khisina et al. 2001). A model of the crystal structure of Hy-2*a* has been proposed as a 2*a*-superstructure of olivine with one Me^{2+}-vacant octahedral layer in the (1 0 0) plane per Hy-2*a* unit cell (Khisina and Wirth 2002). In the present study the crystal structure of Hy-2*a* hydrous olivine is optimized by ab initio calculations. The aims of this study are: (1) verification of the suggested models of Hy-2*a* hydrous olivine structure; (2) calculation of the most stable configurations for Hy-2*a* structure with minimum static lattice energy, by assuming a possible formation of Me^{2+} vacancies in either M1 or M2 octahedral sites; (3) determination of the position of protons and hydrogen bonds in the Hy-2*a* structure. Several different possible configurations of the Hy-2*a* structure are optimized. The results support the idea of a stable olivine structure with ordered planar-segregated OH-bearing defects oriented parallel to (1 0 0). The data obtained indicate a preferred stability of the Hy-2*a* structure with the protons associated with M1 vacancies and bonded with O1 and O2 oxygen sites. The relative energy values of the optimized Hy-2*a* structure configurations correlate as a rule with the average shifts of atoms from their positions in pure forsterite structure.

Keywords Hydrous olivine · Water in nominally anhydrous minerals · Hydrogen bonds · Ab initio quantum mechanics structure refinement · DHMS phases

S. V. Churakov (✉) · R. Wirth
GeoForschungsZentrum Potsdam,
Telegrafenberg, Potsdam, 14473 Germany

N. R. Khisina
Institute of Geochemistry and Analytical Chemistry,
RAS, Kosygin 16, 117957 Moscow, Russia

V. S. Urusov
Moscow State University, Vorob'evi gori,
119899 Moscow, Russia

Present address: S. V. Churakov
CSCS – Centro Svizzero
di Calcolo Scientifico, Galleria 2,
Via Cantonale, 6928 Manno, Switzerland
Tel.: +41-91-610 8222
Fax: +41-91-610 8282
e-mail: churakov@cscs.ch

Introduction

Point defects affect the optical, elastic and chemical properties of minerals. In particular, they facilitate the incorporation of water in nominally anhydrous phases. This aspect is relevant for the problem of fluid storage in the Earth's mantle and the deep crust. The presence of water in nominally anhydrous phases such as olivine may influence the dynamics of the Earth's upper mantle and lithosphere.

FTIR studies have shown that natural olivines usually contain OH groups, although concentration of the latter is very low (Beran and Putnis 1983; Freund and Oberheuser 1986; Kitamura et al. 1987; Miller et al. 1987; Bai and Kohlstedt 1993; Young et al. 1993; Libowitzky and Beran 1995; Kohlstedt et al. 1996; Khisina et al. 2001). The largest OH concentrations such as $n \times 10^{-3}$ wt% have been determined in mantle olivines from kimberlites (Miller et al. 1987). To understand the behaviour of OH-bearing olivines under mantle *P*–*T* conditions, as well as to predict a possible role of the olivine hydration–dehydration processes in subduction zones and the mantle rheology, the mechanism of OH incorporation into the olivine structure should be known.

Hydrogen atoms can be incorporated into the olivine structure by forming either octahedral (M1 or M2) or tetrahedral (Si) vacancies. As hydrogen concentrations are very low in olivines, diffraction methods fail when used for the determination of the crystallographic positions of hydrogen atoms in olivine structure.

This determination can be done by using: (1) IR spectroscopy and (2) by ab initio calculations. Libowitzky and Beran (1995) interpreted IR spectra of olivine on the basis of the pleochroic scheme assuming that vacancies exist on Si and Mg sites. They suggested that (1) the O1 atom is partially replaced by OH defects pointing to a vacant Si site; (2) the O3 atom is a donator oxygen of OH dipoles lying near the O3–O1 tetrahedral edge or roughly pointing to a vacant M2 site; (3) the O2 atom can act as a donator oxygen of an OH group oriented along the O2–O3 edge of a vacant M1 octahedron. Semi-empirical molecular orbital calculations and ab initio calculations of isolated point defects in dry olivine suggest that the M1 vacancies are energetically more favourable than M2 (Lasaga 1981; Brodholt 1997) and much more favourable than Si vacancies (Wright and Catlow 1994; Brodholt 1997). However, in OH-bearing olivine, the energetic relations can be different. In "wet" olivine Si vacancies represent the lower energy configuration (Brodholt and Refson 2000). Furthermore, the energetic relations for groups of ordered defects are unknown and further calculations are necessary.

Recently, nanometre-sized OH-bearing inclusions were found in natural forsterite (Fo_{82}) from the mantle peridotite nodule 9206, Udachnaya kimberlite pipe (Khisina et al. 2001; Khisina and Wirth 2002). The origin of these inclusions has not been clarified until now. These inclusions are characterized by a superperiodicity of the olivine lattice in the SAED patterns and a periodic band-like contrast in HRTEM images. Based on HRTEM, SAED, AEM and EELS data it was concluded that OH-bearing inclusions have a cation-deficient olivine-like structure with Me^{2+} vacancies (denoted as □) located in either (1 0 0) or (0 0 1) octahedral layers of the olivine structure. These vacancy-bearing octahedral layers form ordered arrays of periodic planar defects (PD) in the olivine structure. Such a structure was named hydrous olivine (Khisina et al. 2001). The (1 0 0) PDs in hydrous olivine show a periodicity along the *a* direction of olivine, $2d_{(1\,0\,0)}$ (Hy-2*a* polymorph) or $3d_{(1\,0\,0)}$ (Hy-3*a* polymorph); the (0 0 1) PDs are characterized by a $3d_{(0\,0\,1)}$ periodicity along the *c* direction of olivine (Hy-3*c* polymorph). The chemical compositions of the inclusions are $Mg_{1.615}Fe^{2+}_{0.135}\square_{0.25}SiO_4H_{0.5}$ (Hy-2*a*) and $Mg_{1.54}Fe^{2+}_{0.12}\square_{0.33}SiO_4H_{0.66}$ (Hy-3*a* and Hy-3*c*) (Khisina and Wirth 2002). The crystal structure of hydrous olivine was suggested to be a modular olivine structure with Mg-vacant modules. The crystal-chemical formulae of hydrous olivines in terms of a modular structure were proposed as $[MgH_2SiO_4]\cdot 3[Mg_{1.82}Fe_{0.18}SiO_4]$ for Hy-2*a* and $[MgH_2SiO_4]\cdot 2[Mg_{1.82}Fe_{0.18}SiO_4]$ for Hy-3*a* and Hy-3*c* (Khisina and Wirth 2002). It was found that Hy-2*a* hydrous olivine is similar to phase D, which was synthesized by Liu (1987) at high pressure-high temperature conditions. Phase D by Liu and Me^{2+}-vacant modules in hydrous olivines are the same with respect to the chemical composition. Powder diffraction data obtained by Liu (1987) for phase D can be indexed in terms of the Hy-2*a* unit cell (Khisina and Wirth 2002). Because Hy-2*a* hydrous olivine is found in mantle material and looks similar to the high-pressure phase D, Hy-2*a* might be considered as an OH-bearing mineral phase, which is stable in the upper mantle. Therefore, it is important to refine the Hy-2*a* crystal structure with respect to the location of the hydrogen atoms. However, the nanometre-sized hydrous olivine inclusions are too small for any crystal structure determinations. Therefore, a first-principles quantum mechanic investigation seems to be the only way to refine the crystal structure of the Hy-2*a* hydrous olivine.

In this paper we present the results of ab initio structure optimization of the Hy-2*a* hydrous olivine, based on the crystal chemical model suggested earlier by Khisina and Wirth (2002). The purpose of this study was (1) to verify the validity of the initial model; (2) to obtain the most stable configuration of hydrogen atoms in the Hy-2*a* structures, which have the minimum static lattice energy, by assuming a possible formation of Me^{2+} vacancies in either M1 or M2 octahedral sites. Ab initio structure optimizations on the Hy-3*a* and Hy-3*c* olivines, as well as data on dynamic stability of simulated structures, are subject of ongoing research.

The results reported here show that the structure with the hydrogen atoms bonded to O1 and O2 ligands around the M1 cation vacancies seems to be the most stable relative to the other possible configurations.

Prerequisites and starting constraints

According to the model of the hydrous olivine structure (Khisina and Wirth 2002), the Hy-2*a* cell is considered as a 2*a* superstructure of olivine with one (1 0 0) Me^{2+}-vacant octahedral layer per two unit cells of olivine (or equivalently per one unit cell of Hy-2*a*). Such a structure can be modelled assuming either M1 or M2 vacancies in the (1 0 0) plane. Consequently, two sets of the refinement procedures were performed, by assuming either all M1 or all M2 sites to be vacant in the given (1 0 0) octahedral layer.

The orthorhombic unit-cell parameters of Hy-2*a* were assumed to be equal to those observed experimentally by Khisina and Wirth (2002): $a_{Hy2a} = 2a_{Ol} = 9.524$ Å; $b_{Hy2a} = b_{Ol} = 10.225$Å; $c_{Hy2a} = c_{Ol} = 5.994$ Å; $\alpha = \beta = \gamma = 90°$. These parameters were kept constant during the structure optimization and only the atomic positions were allowed to change. The calculations were carried out on iron-free Hy-2*a* hydrous olivine with the chemical composition $(MgH_2SiO_4)\cdot 3(Mg_2SiO_4)$. To obtain the most stable structure of Hy-2*a* olivine or, in other words, to find the structure with minimum static lattice energy, numerous structure optimizations of different initial configuration with either M1 or M2 vacancies ordered in the (1 0 0) plane were performed. In the case of structures with M2 vacancies, the initial coordinates of hydrogen atoms were taken within the vacant M2

octahedra. For structures with M1 vacancies we tried to stabilize hydrogen atoms in two different modes: (1) within vacant M1 octahedra; (2) within both vacant M1 octahedra and interstitial sites.

Methodology

Static 0 K structure optimizations have been carried out using the CPMD-3.4.1 density functional (DFT) code (Hutter et al. 1995–2001). The calculations were accomplished with the BLYP exchange-correlation functional (Becke 1988; Lee et al. 1988) utilizing the generalized gradient approximation (GGA). Non-local norm-conserving Goedecker-type pseudopotentials (Goedecker et al. 1996) have been applied to account for core electrons. Valence electron orbitals were approximated by plane-wave expansion, with a 950-eV plane-wave energy cutoff. The valence electron states for Mg, Si, O and H were $2s^2 2p^6 3s^2$, $3s^2 3p^2$, $2s^2 2p^4$ and $1s^1$, respectively. A $1 \times 1 \times 2$ supercell containing 116 atoms ($Mg_{28}H_8Si_{16}O_{64}$) was used in the calculations.

A relaxation of atomic positions was allowed and the lattice energy calculations were performed in two steps. First, optimal positions of atoms were found using a Γ-point sampling. Then, the energy of supercell with optimized atomic positions was calculated on $2 \times 2 \times 2$ Monkhost–Pack mesh (Monkhorst and Pack 1975), using eight k points with inversion symmetry.

To test the accuracy of geometry convergence in respect to the k-point mesh, the structure C5 (see Fig. 1a and text for details) was optimized applying energy integration over eight k points. Maximal atomic displacement was less than 0.004 Å. The corresponding energy difference was only 0.0005 eV/formula, which is at least 1 order of magnitude lower than the smallest energy difference for various configurations of H atoms (see Table 1). The accuracy of the geometry calculations in respect to the basis set has been tested on isolated molecules: MgO, SiO and H_2O. The calculations show that absolute convergence of the energy is achieved for the plane-wave cutoff above 2000 eV. The bond lengths predicted with 950 eV cutoff are in 2.5, 0.5 and 2.0% agreement with values obtained at 2500 eV. The corresponding bonds energy difference was within 3%. The absolute uncertainties can be as high as 0.05 eV.

It should be emphasized again that the structure optimizations have been carried out for a fixed size and orthorhombic geometry of the supercell. This is a rather strong restriction because a lattice energy of the studied structures can be reduced by deforming the geometry of the unit cell. Alternatively, the calculations could be done for fixed pressure with variable cell geometry. This would demand absolute convergence of the lattice energy and stress with respect to the plane-wave cutoff and k-points mesh. Because of limitation of computer power, such calculations cannot be done.

Fixing lattice parameters, the other limitations of DFT calculations can be avoided. In particular, DFT does not take into account the dispersion interaction between molecules and atoms. In our systems, these forces can play an important role in the plane of defects. The other source of uncertainties is the exchange-correlation functional. The DFT calculations are known to systematically over- or underestimate lattice parameters of solids by a few percent, if LDA or GGA approximations are used, respectively. Although the LDA calculations for magnesium silicates (e.g., Karki et al. 1997) give the unit-cell volume and elastic constants almost within the experimental uncertainty, the GGA approximation is proved to be best exchange-correlation functional among others to predict hydrogen bonding (Sprik et al. 1996). Moreover, this functional has been successfully used to predict proton mobility in different polymorphs of the Mg_2SiO_4 (Heiber et al. 1997).

To summarize, the main delicacy of these calculations was to determine energy difference among the isochemical structures having the difference in the geometry of OH bonds. This task can be solved with low number of k points and relatively small cutoff below absolute convergence of energy. We expect the bond geometry to be in better than 3% agreement with experimental values. The errors in the energy calculations (the difference in the energy between obtained structures) are below 0.05 eV.

Results

The resulting static lattice energy values, the corresponding space groups of symmetry and hydrogen bond parameters for a number of optimized structure models are given in Table 1. The corresponding three-dimensional models of optimized structures are shown in Figs. 1, 2 and 3.

Hy-2*a* structure with M1 vacancies

H atoms associated with M1 vacancies in (0.5, 0.0, 0.0) and (0.5, 0.0, 0.5)

The M1 octahedra are formed by two O1, two O2 and two O3 oxygen atoms. Therefore, for H atoms entirely located in the M1 vacancy, several configurations with different structures and energies are possible. The three-dimensional models of optimized structures with M1 vacancies (structures C5, C8, C2, C6, C4) are shown in Fig. 1. The data of the static lattice energy, hydrogen bond lengths and angles as well as H distances and O–H angles for the optimized atomic configurations are summarized in Table 1.

The lowest energy was found for the structure C5, where two H1 and two H2 protons are forming O–H-donating bonds with O1 and O2 oxygen atoms, respectively (Fig. 1a; Table 1). The O2–H2 bond vector is directed approximately perpendicular to the PD plane, whereas the O1–H1 bond vector is almost parallel to the PD plane. There are two distinct hydrogen bonds observed, both bifurcated, O2–H2...(O3/O1) and O1–H1...(O2/O3). One and the same O2 atom is involved in both bifurcated hydrogen bonds; every O3 oxygen of the M1-vacant polyhedron is implicated in one O...H contact (Fig. 1a). The O1 and O2 atoms participate in both O–H and O...H bonds.

The structure C8 (Fig. 1b) is only 0.014 eV/formula higher in energy than the C5 configuration (Table 1). Two H2 and two H3 atoms form two O2–H2...O1 and two O3–H3...O1 hydrogen bonds, respectively (Fig. 1). One and the same O1 atom is involved in both O3–H3...O1 and O2–H2...O1 hydrogen bonds, thus joining them into O3–H3...O1...H2–O2 chain (Fig. 1b). O2 and O3 atoms form one O–H donating bond each, while every O1 atom is involved in two O...H bonds.

The C2 structure (Fig. 1c) is just 0.044 eV/formula higher in energy than the C5 configuration (Table 1). Two of four protons form two O2–H2...(O3/O1) bifurcated hydrogen bonds. Two other hydrogen atoms participate in two O1–H1...(O3/O2) bifurcated bonds. Thus, in the C2 configuration the O1 oxygen acts as an

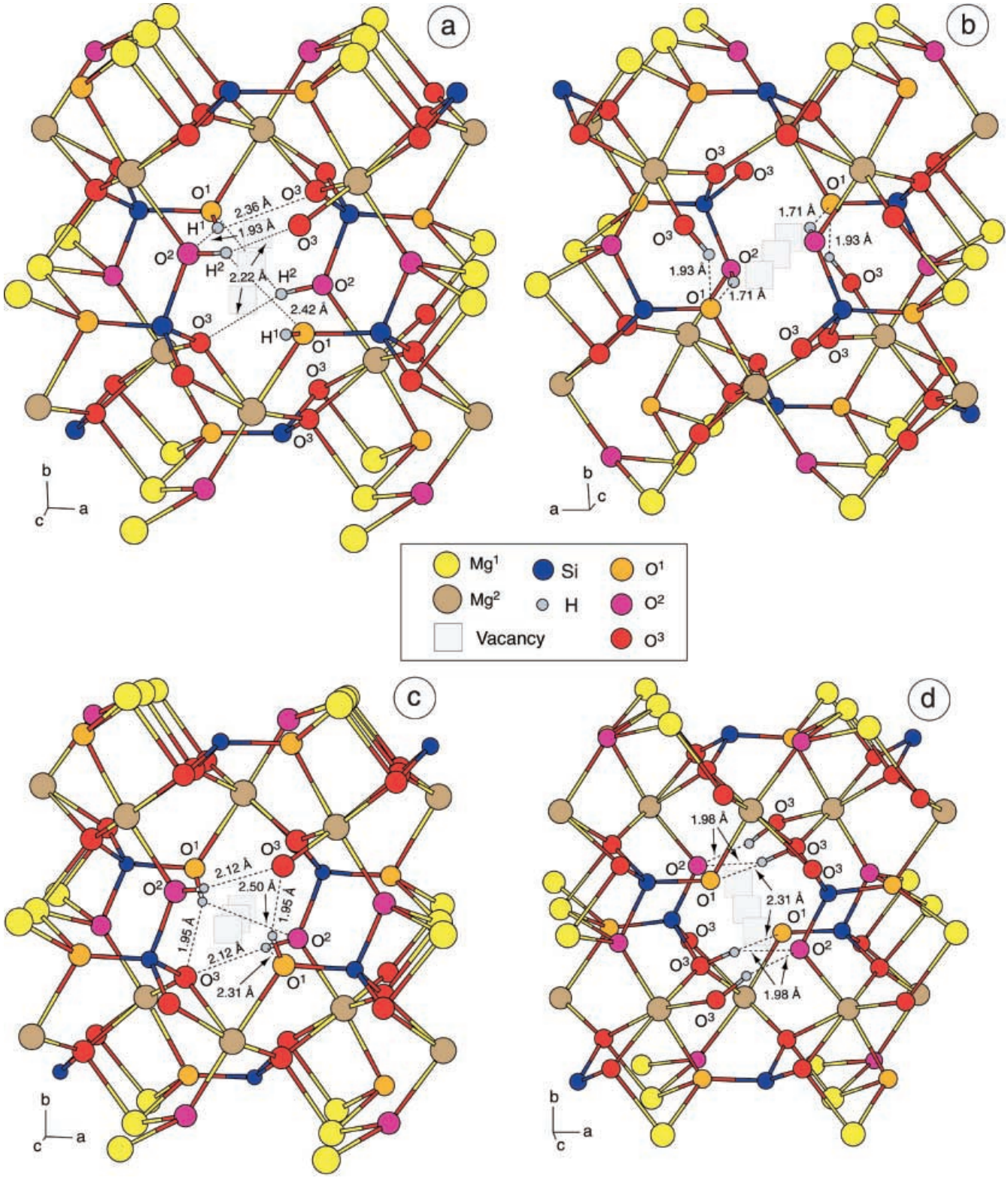

Fig. 1a–e Contd.

acceptor. The O2 oxygen atoms participate in one accepting and one donating bond. One of two O3 oxygen atoms in the first coordination shell around M1 vacancy is an electron donor in two distinct hydrogen bonds while another O3 is not involved in hydrogen bonding (Fig. 1c.).

The C6 structure (Fig. 1d) is 0.300 eV/formula higher in energy than the C5 (Table 1). All hydrogen atoms are

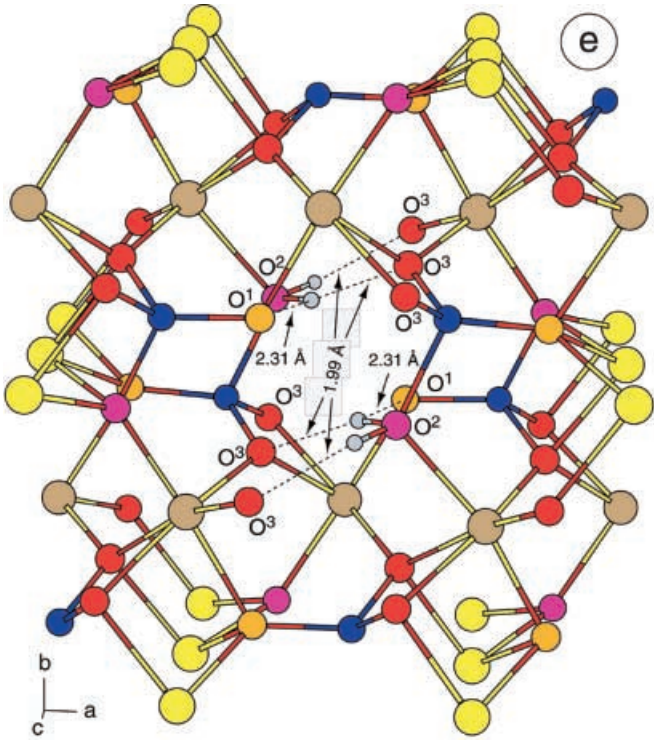

Fig. 1a–e Three-dimensional models of optimized Hy-2*a* crystal structures bearing M1 vacancies and H atoms located within vacant M1 polyhedra. **a** C5 configuration; hydrogen atoms participate in O2–H2...(O3/O1) and O1–H1...(O2/O3) hydrogen bonds. **b** C8 configuration, hydrogen atoms participate in O3–H3...O1 and O2–H2...O1 hydrogen bonds. **c** C2 configuration, hydrogen atoms participate in O1–H1...(O3/O2) and O2–H2...(O1/O3) hydrogen bonds. **d** C6 configuration, hydrogen atoms participate in O3–H3...(O1/O2) hydrogen bonds. **e** C4 configuration, hydrogen atoms participate in O3...H2–O2–H2...O1 bonds

bonded to O3 atoms forming O3–H3 donating bonds. There are four equivalent bifurcated hydrogen bonds O3–H3...(O1/O2) (Fig. 1d).

The C4 configuration possesses the highest energy in a series of structures having protons associated with M1 vacancies (Fig. 1e; Table 1). While the supercell energy is rather high (about 0.875 eV/formula relative to C5 configuration), this structure is of particular interest because it contains water-like H–O–H complexes. Thus, every O2 forms two O–H bonds with hydrogen atoms (O2–H2 = 1.04 Å). The shortest H...H distance is about 1.625 Å and the corresponding H–O2–H angle is equal to 103°, which is almost identical to the H–O–H valence angle of the free water molecule (104.5°). The O...H2 contacts are bifurcated into O3...H2 and O1...H2 components.

The O...H contacts in C5, C2, C6 and C4 structure configurations cross the PD plane, so that the hydrogen O–H...O bonds fasten the structure joining two by two tetrahedra situated opposite to each other across the PD plane (Fig. 1a,c,d,e). However, the O...H vectors are aligned with the PD plane in the C8 structure configuration (Fig. 1b).

Interstitial protons

Numerous attempts have been made to stabilize protons in interstitial positions of Hy-2*a* olivine lattice. In most cases, the hydrogen atoms placed initially in interstitials were found to migrate from interstitials towards the nearest M1 vacancies. Only two stable configurations were found, I1 and I2, where two of four protons are located in interstitials. The corresponding three-dimensional models of optimized structures are shown in Fig. 2.

In the I1 structure (Fig. 2a) two protons are located in vacant M1 polyhedra, whereas two others are located in M3 interstitials. All H atoms form O–H-donating bonds with O2 atoms pointing to either O1 (H atoms associated with M1 vacancy) or O3 (H atoms associated with M3 interstitial). The energy of the I1 configuration is 1.876 eV/formula larger than the energy of the C5 structure. This is also substantially higher than that of structures with all protons associated to Me^{2+} vacancies, either M1 or M2.

In I2 configuration (Fig. 2b) two protons are located in a vacant M1 polyhedron, while two others are located in M4 interstitials. The interstitial protons in I2 are bonded to the oxygen atoms that participate in the first coordination shell around M1 vacancies. Those H atoms which are located in M4 interstitials form O3–H3...(O2/O3) bifurcated hydrogen bonds. Those H atoms which are located in a vacant M1 polyhedron form O2–H2...O1 hydrogen bonds. The energy of the I2 configuration, being 0.815 eV/formula relative to the C5 structure (Table 1), is substantially smaller than that of I1.

The energy values obtained for I1 and I2 exceed that of C5 rather markedly (Table 1) and they are unlikely to be overstepped by entropy effects. Therefore, a probability for such proton locations to occur should be extremely low and no further attempts have been taken to stabilize structures with interstitial protons.

Hy-2*a* structure with M2 vacancies

Three-dimensional optimized configurations of Hy-2*a* olivine with protons associated with M2 vacancies (D4, D3, D1) are shown in Fig. 3. Selected parameters of hydrogen bonds and lattice energy are summarized in Table 1.

The most favourable structure configuration with M2 vacancies (Fig. 3a) has energy which is 0.593 eV/formula larger than that of the optimal configuration C5 (Table 1). In the D4 structure all protons are bonded to O3 atoms forming four O3–H3...O3 hydrogen bonds per unit cell (Fig. 3a). The two O3 atoms participating in one and the same hydrogen bond belong to different tetrahedra, so that every Si tetrahedra near a vacant M2 site has one O3 involved in the O3–H3 bond and another O3 involved into the O3...H3 contact. Proton position H3 is split into H3′ and H3″, so that the corresponding O3...H3′ and O3...H3″ bond lengths are different.

Table 1 Relative energies of some optimized Hy-2*a* olivine structures and various geometry parameters of the hydrogen bonds corresponding to different locations of protons. The absolute value of the static lattice energy for C5 structures is taken to be zero

Proton location	Associated with M1 vacancy					Associated with M2 vacancy			Protons in M1 vacancy and interstitial	
Configuration	C5	C8	C2	C6	C4	D4	D3	D1	I2	I1
ΔE, eV/f.u.[a]	0.000	0.014	0.044	0.300	0.875	0.593	0.617	1.156	0.815	1.826
Symmetry	$P2_1$	$P\bar{1}$	$P2_1$	$P2_1/m$	$P2_1/m$	$P\bar{1}$	$P2_1/m$	$P2_1$	$P\bar{1}$	$P2_1$
Δ,[b] Å	0.060	0.094	0.072	0.117	0.093	0.074	0.130	0.112	0.090	0.124
H1–O1, Å[c]	$^{(x2)}$1.01		$^{(x2)}$1.01					$^{(x2)}$1.01		
H2–O2, Å	$^{(x2)}$1.00	$^{(x2)}$1.03	$^{(x2)}$1.00		$^{(x4)}$1.04			$^{(x2)}$1.00	$^{(x2)}$1.06	$^{(x2)}$1.04 $^{(x2)}$1.01
H3–O3, Å		$^{(x2)}$1.02		$^{(x4)}$1.02		$^{(x2)}$1.00 $^{(x2)}$1.02	$^{(x4)}$1.03		$^{(x2)}$1.01	
H1···O2, Å	$^{(x2)}$1.93		$^{(x2)}$2.50							
H1···O3, Å	$^{(x2)}$2.36		$^{(x2)}$1.95					$^{(x2)}$2.14 $^{(x2)}$2.26		
H2···O1, Å	$^{(x2)}$2.42	$^{(x2)}$1.71	$^{(x2)}$2.31		$^{(x4)}$2.31				$^{(x2)}$1.60	$^{(x2)}$2.43 $^{(x2)}$1.86
H2···O3, Å	$^{(x2)}$2.22		$^{(x2)}$2.12		$^{(x4)}$1.99			$^{(x2)}$2.31 $^{(x2)}$2.23		$^{(x2)}$1.60
H3···O1, Å		$^{(x2)}$1.93		$^{(x4)}$2.31		$^{(x2)}$2.47	$^{(x2)}$2.42			
H3···O2, Å				$^{(x4)}$1.98		$^{(x2)}$2.33 $^{(x2)}$2.39			$^{(x2)}$2.39	
H3···O3, Å						$^{(x2)}$2.12 $^{(x2)}$1.89	$^{(x2)}$1.76		$^{(x2)}$1.88	
H1-□, Å	1.27		1.21					1.13		
H2-□, Å	1.33	1.26	123		1.17			1.09	1.28	2.90
H3-□, Å		1.16		1.19		1.21	1.27			
H–H, Å	2.17	2.42	1.88	2.37	1.61	2.41	2.50	2.18	3.22	3.40
O1–H1-□, °	125		135					154		
O2–H2-□, °	124	113	128		126			163	109	115
O3–H3-□, °		121		127		140	119			
O1–H1···O2,°	152		113							
O1–H1···O3,°	104		154					128 121		
O2–H2···O1,°	115	157	120		124				161	147 111
O2–H2···O3,°	163		158		152			120 125		165
O3–H3···O1,°		148		102		115	114			
O3–H3···O2,°				158		115 123			117	
O3–H3···O3,°						132 146	150		141	

[a] f.u. = formula unit
[b] Atomic displacements averaged over all atoms in Hy-2*a* unit cell
[c] A number of a given bond contact per one Hy-2*a* unit cell is indicated in brackets

A somewhat higher energy was obtained for the structure D3 (Fig. 3b). Again, as in the D4 structure, all H atoms are bonded to O3 atoms and every two O3 atoms participating in one and the same hydrogen bond belong to different tetrahedra. However, in contrast to the D4 structure, two O3 atoms from one and the same tetrahedron are involved in two different O3–H3 bonds, which form H3...O3 contacts of 1.76 Å in length with O3 atoms of the other SiO_4 tetrahedron.

Finally, the D1 structure with protons bonded to O1 and O2 (Fig. 3c) was obtained. There are two kinds of bifurcated hydrogen bonds, O1–H1...(O3/O3) and O2–H2...(O3/O3), and every O3 atom participates in both of them (Fig. 3c).

Discussion

A probable symmetry of hydrous olivine

Olivine is characterized by an orthorhombic *Pbnm* space group. Modifying the structure by doubling the cell in the *a* direction and by removing all the M1 atoms in the (1 0 0) plane, the glide planes *b*, *n* and the corresponding two-fold screw axes in the (0 0 1) plane are lost. Similar symmetry elements disappear when M2 vacancies are assumed. Therefore, the highest symmetry of the olivine lattice with doubled lattice parameter corresponds to a monoclinic $P2_1/m$ space group. However, lowering the

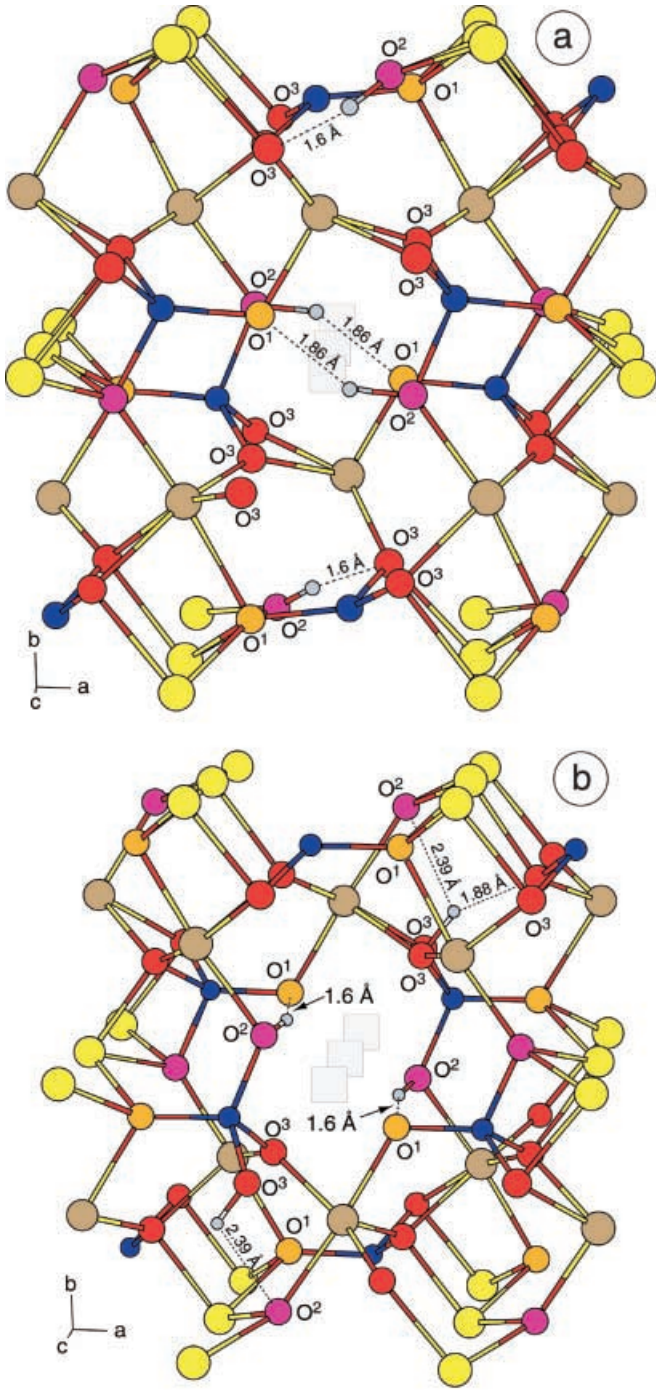

Fig. 2a, b Three-dimensional models of optimized Hy-2*a* crystal structures with H atoms located in both interstitials and vacant M1 polyhedra. In the I2 structure **b** interstitial protons occupy the M4 polyhedron, while the I1 structure **a** is located within M3 sites

symmetry from *Pbnm* to $P2_1/m$ space group causes a splitting of crystallographic sites in hydrous olivine. Thus, the atoms sitting apart from the symmetry elements associated with *n* and *b* glide planes (Mg2, Si, O1, O2, O3) splits into four non-equivalent positions characterized by different coordination environments, which is illustrated for the particular case of C5 structure in the Fig. 4 and Table 3. Because of the special site symmetry of the M1 position in olivine, the Mg1 splits in only two non-equivalent sites [(0, 0, 0) and (1/4, 1/2, 1/2)], one of which has an M1 vacancy in the second coordination shell, and the other no M1 vacancy in the second coordination shell. Further lowering of symmetry and splitting of crystallographic positions is controlled by the orientation of protons (Table 1).

In the C6, C4 and D3 structures protons are located in general positions according to $P2_1/m$ symmetry. In the C5, C2, D1 and I1 configuration the orientation of protons violates the mirror plane and the resulting structure symmetry is lowered to the $P2_1$ space group. Finally, only inversion symmetry is present in C8, D4 and I2 configurations. The symmetry lowering in the C5, C8, C2, D4, D1, I1 and I2 structures induces further splitting of crystallographic positions. In particular, there are two non-equivalent positions occupied by protons.

The resulting loss of symmetry elements, specific for the orthorhombic space group *Pbnm*, reduces the Hy-2*a* symmetry down to monoclinic $P2_1/m$ (C6, C4, D3) or $P2_1$ (C5, C2, D1, I1) and even triclinic $P\bar{1}$ (C8, D4, I2). This means that the Hy-2*a* unit cell deviates in shape from the initially imposed orthogonal metrics.

The lowest-energy Hy-2*a* structures

The energy difference between all ten optimized structure configurations (Table 1) is rather small. In particular, the energy difference between C5, C8 and C2 structures is almost within the accuracy of the calculations. This might indicate that all these configurations coexist at high temperatures. However, the C5 configuration shows the minimum energy (Table 1) and may represents the most stable structure of Hy-2*a* annealed to low temperatures. It is also correlated with the lowest value of average atomic shifts (Table 2) with respect to an optimized forsterite structure. The C5 structure is discussed in detail to show the main structure changes in olivine due to the incorporation of hydrogen.

The Hy-2*a* structure is thought of as formed by alternated modules with Mg_2SiO_4 and MgH_2SiO_4 composition (Khisina and Wirth 2002); the latter are shown as shadowed in grey in Fig. 4. In the Hy-2*a* optimized structure there are hydrogen bonds O1–H1...O2 and O2–H2...O3 joining two by two the Si^A and Si^C tetrahedra (see Fig. 4). H1 and H2 are situated inside vacant M1 octahedra which are arranged to form a ''wall'' of M1 vacancies in (1 0 0) plane, i.e., forming a planar defect (Fig. 4).

The presence of OH^- in the first coordination shell of Mg(M2) and Si atoms shifts them from their original positions. As a result, the structural positions of Si and Mg(M2) split. M2 positions split into four subpositions, indicated as $M2^I$, $M2^{II}$, $M2^{III}$ and $M2^{IV}$ (Fig. 4; Table 3), with different neighbours in the first and second coordination shells (Table 3). Si positions also split

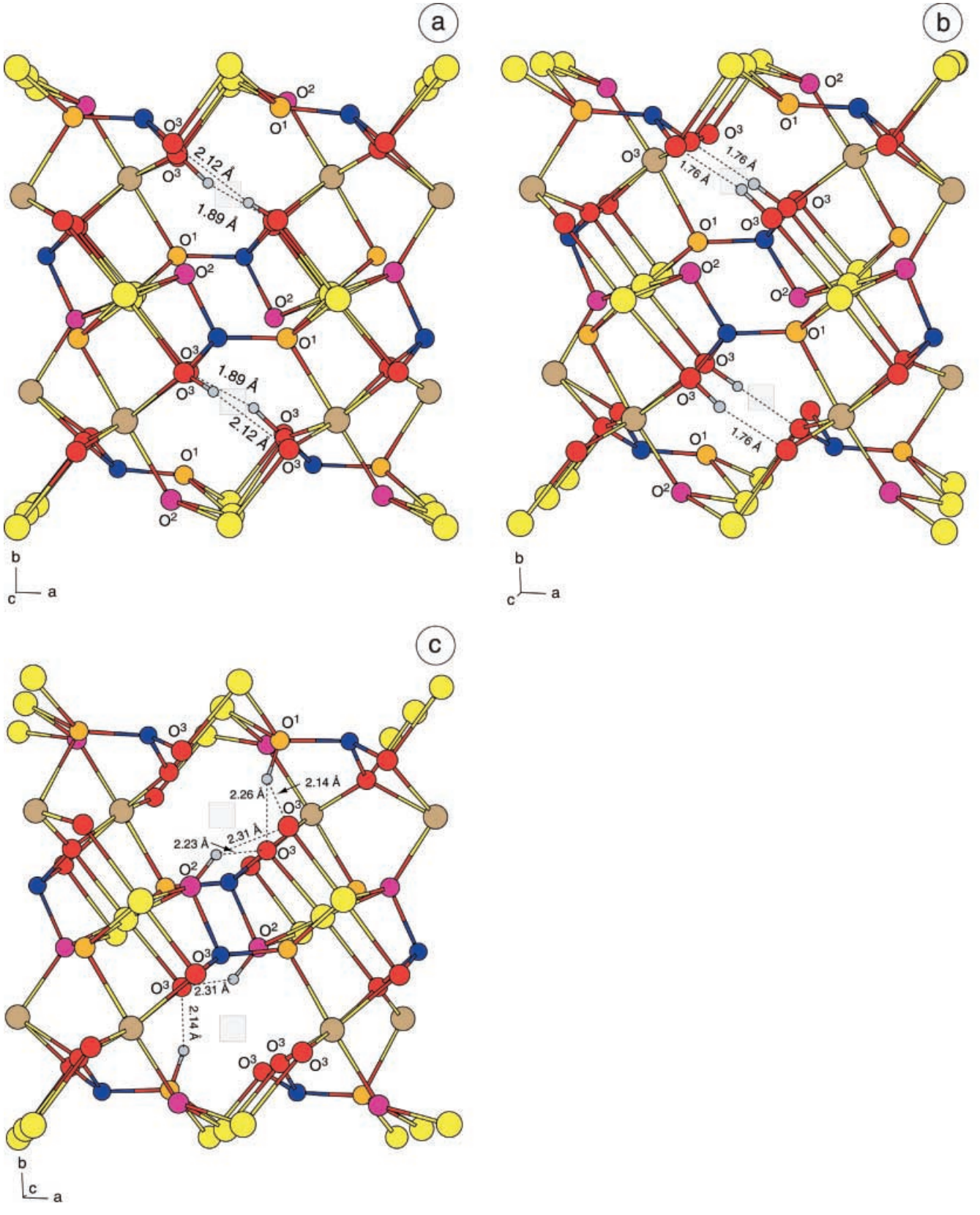

into four subpositions, labelled Si^{A}, Si^{B}, Si^{C} and Si^{D} (Fig. 4; Table 3). $M2^{II}$ and Si^{D} atoms are in the planar defect plane; $M2^{I}$ and $M2^{III}$, Si^{A}, Si^{B} and Si^{C} are outside the planar defect (Table 3; Fig. 4). This is obvious from the (1 0 0) projection of the Hy-2*a* structure (Fig. 4). The most significant shifts are observed for Si atoms,

◄

Fig. 3a–c Three-dimensional models of optimized Hy-2*a* crystal structures bearing M2 vacancies and H atoms located within vacant M2 polyhedra. **a** D4 configuration, hydrogen participates in O3–H3′…O3 and O3–H3″…O3 hydrogen bonds. **b** D3 configuration, hydrogen participates in O3–H3…O3 hydrogen bonds. **c** D1 configuration, hydrogen participates in O1–H1…(O3/O3) and O2–H2… O3/O3) bifurcated bonds

Mg atoms in M2 and oxygen atoms in O1 and O2 positions. The largest shifts for Mg in the $M2^{I}$ and $M2^{III}$ sites are observed along the *b* direction of the structure, while $M2^{IV}$ is shifted in the *a* direction. Small shifts in the *c* direction can be observed for $M2^{IV}$ and $M2^{II}$ (Fig. 4). Oxygen atoms in the O1, O2 and O3 sites are shifted approximately in [1 1 1] and [1 $\bar{1}$ 1] directions. The O1 and O2 are much more extensively shifted than O3. Si atoms in Si^{A} and Si^{C} sites are shifted to a greater extent than Si^{D} and Si^{B}.

How reasonable are the minimum energy structure configurations C5, C8 and C2?

The calculated energy differences for various configurations of proton associated with an Me^{2+} vacancy are in agreement with general crystal-chemical arguments. In the olivine structure the M1 octahedral environment is formed by two O1, two O2 and two O3 atoms. Every oxygen in the olivine structure is bonded to one Si and three Mg atoms; every O3 atom has one bond with Mg in the M1 site and two bonds with two Mg in the M2 sites, whereas the O1 and O2 atoms bound with two Mg(M1) and with one Mg(M2). The Pauling's bond strengths of Mg and Si atoms are 1/3 v.u. and 1 v.u., respectively. Therefore, any [0 0 1] chain of M1 vacant octahedra produces unsaturated valence of about −2/3 v.u. on O1 as well as on O2 atoms and only of −1/3 v.u. on O3 oxygen atoms. Therefore, the structures with H atoms bonded to O1 and O2 atoms are expected to be energetically favourable, and O3 atoms are involved in H...O contacts. This is consistent with C5 and C2 structure configurations. In the C8 structure there are two very short H2...O1...H3 bonds which can be comparable to an O1–H bond.

The C8 and C2 structures can be easily constructed starting with the C5 configuration. Thus, the rotation of the O1–H1 dipole from [0 0 1] to [0 1 0] direction is basically sufficient for the C2 structure to be formed. The C8 configuration can be simulated by rotating the O1–H1 dipole from the [0 0 1] to [0 1 0] direction followed by proton transfer reaction: O1–H...O3⇒O1...H–O3 and rotation of the O2–H2 dipole from the [1 0 0] to [0 1 0] direction. Such a relatively simple mechanism of the structure transformation and a very low energy difference suggest that the C2 and C8 structures are to be considered as competitors to the C5 configuration.

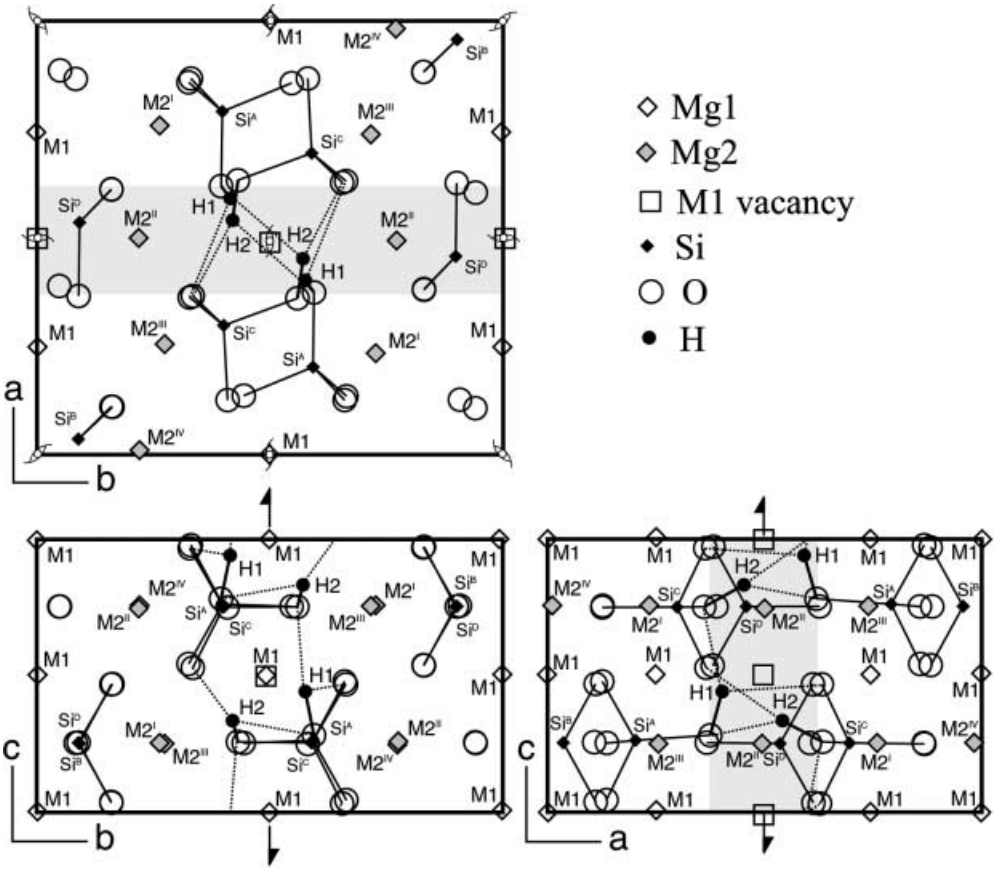

Fig. 4 (0 1 0) [a], (1 0 0) [b] and (0 0 1) [c] projections of the lowest-energy structure geometry (C5) for Hy-2*a*. The symmetry elements of the $P2_1$ space group are indicated. Non-equivalent positions of M2 cation sites are denoted by *Roman digits*; split Si sites are labelled by *letters*. H1 and H2 hydrogens are bonded to O1 and O2 oxygen atoms, respectively. The structural module MgH_2SiO_4 is *shadowed in grey*

Table 2 Average atomic displacements relative to the optimized structure of forsterite for different optimized configurations of Hy-2*a* olivine structure with M1 vacancies

Configuration	C5	C8	C2	C6	C4
$\Delta_{Mg(1)}$, Å	0.050	0.058	0.053	0.075	0.065
$\Delta_{Mg(2)}$, Å	0.073	0.101	0.082	0.103	0.103
Δ_{Mg}, Å	0.063	0.082	0.069	0.091	0.087
Δ_{Si}, Å	0.067	0.065	0.073	0.151	0.086
$\Delta_{O(1)}$, Å	0.093	0.083	0.079	0.124	0.095
$\Delta_{O(2)}$, Å	0.052	0.113	0.076	0.134	0.132
$\Delta_{O(3)}$, Å	0.041	0.114	0.067	0.111	0.083
Δ_{O}, Å	0.057	0.106	0.072	0.120	0.098
Δ, Å	0.060	0.094	0.072	0.117	0.093

Table 3 The nearest neighborhood for Mg in M2 sites and Si atoms in the first and second coordination shells (C5 configuration)

Atom	First coordination shell	Second coordination shell
$M2^{Ia}$	O2–H2; O1; 4O3	4M1; $M2^{IV}$; $M2^{II}$
$M2^{II}$	O1–H1; O2; 4O3	4v(M1); $M2^{III}$; $M2^{I}$
$M2^{III}$	O2; O1; 4O3	4M1; $M2^{II}$; $M2^{IV}$
$M2^{IV}$	O2; O1; 4O3	4M1; $M2^{I}$; $M2^{III}$
Si^{A}	O1–H1; O2; 2O3	Outside the $[MgH_2SiO_4]$ module
Si^{B}	O1; O2; 2O3	
Si^{C}	O2–H2; O1; O3; O3···H2	
Si^{D}	O2; O1; 2O3	Belongs to the $[MgH_2SiO_4]$ module

[a] See indication in the Fig. 4

Although the orthogonal cell of the Hy-2*a* hydrous olivine was constrained in the calculations, the resulting loss of symmetry elements required by orthorhombic space groups must cause a declination of the Hy-2*a* unit cell from orthogonal metrics. However, such lowering of the symmetry, from orthorhombic *Pbnm* in olivine to monoclinic $P2_1$ in C5, is locally caused and the charge mismatch due to the cation defects is partly compensated for by the hydrogen bonds. Therefore, it is reasonable to assume that the β angle of the fully relaxed Hy-2*a* lattice should be rather close to 90°. This means that the orthogonal lattice metric constrained by the model should not lead to any significant errors in the calculations. Moreover, in the natural samples, the Hy-2*a* phase was observed to occur in the form of nanometre-sized inclusions enclosed in the host olivine. Under these circumstances, the Hy-2*a* unit cell is forced by the olivine structure to keep its orthogonal shape. Therefore, the calculations with the constrained orthorhombic unit cell seem to mimic conditions existing in natural samples in the best possible way.

Conclusions

Probable crystal structures of Hy-2*a* hydrous olivine $(MgH_2SiO_4)\cdot 3(Mg_2SiO_4)$ were predicted by using ab initio calculations. An energy difference for several Hy-2*a* structure configurations with hydrogen atoms located either in M1 or M2 vacancies or both in M1 vacancies and interstitial positions was determined. The calculations predict a preferential stability of structures with hydrogen atoms associated with M1 vacancies relative to M2 vacancies or interstitial sites. The structures with the M2 vacancies are comparable in energy with some configurations where protons are located both in the M1 vacancies and interstitial sites. The lowest energy was found for a Hy-2*a* structure with the C5 configuration, where the cation vacancies are formed in M1 octahedral sites and all the hydrogen atoms are located in M1 vacancies, thus forming two bifurcated hydrogen bonds, O1–H1...(O2/O3) and O2–H2...(O1/O3). Two structures with slightly higher energies characterized by short hydrogen bonds O2–H2...O1 and O3–H3...O1 (C8) and bifurcated hydrogen bonds O2–H2...(O3/O1) and O1–H1...(O3/O2) (C2) were found, and therefore should be present in natural samples.

The data obtained demonstrate a mode of H-atom incorporation in the structure of olivine, which is a nominally anhydrous mineral. The results support the idea about the existence of a stable olivine structure with ordered planar-segregated OH-bearing defects oriented parallel to (1 0 0) (Khisina and Wirth 2002). A hypothetical model of such a structure (Hy-2*a*) was suggested for nanometre-sized inclusions observed by TEM in a mantle olivine grain. We suggest that the Hy-2*a* hydrous olivine made of C5, C8 and C2 structure fragments is stable at high pressure-high temperature conditions. The arguments are: (1) Hy-2*a* hydrous olivine looks similar to the DHMS phase D synthesized by Liu (1987) at 22 GPa, 1000 °C; (2) the TEM observations give evidence that the Hy-2*a* inclusions had been formed earlier than the 10-Å phase, which filled healed cracks in the same grain. In turn, the 10-Å phase is known to be stable at *P–T* conditions above 3–5 GPa and below 700 °C (Wunder and Schreyer 1997; Chinnery et al. 1999). Therefore, the Hy-2*a* inclusions seem to be formed under *P–T* conditions of the upper mantle. They thus provide evidence for the presence of water in the Earth's upper mantle. It can be expected that hydrous olivine will influence the rheological properties of the mantle. For instance, a possible occurrence of Hy-2*a* olivine in subduction zones can cause low-depth earthquakes. The results obtained should be taken into account for interpretation of geophysical data.

Acknowledgements We are thankful to Prof. Dr. W. Heinrich for his support of this investigation. The discussions with S. Sobolev and L. Dubrowinsky were very constructive. We thank Prof. M. Parrinello, Dr. A. Seitsonen and D. Aktah from the Swiss Center of Scientific Computing for help in the optimal choice of computational methodology and the simulations setup. The investigation was carried out with financial support of the Russian Fund for Fundamental Researchs (99-05-65139 and 00-15-98582), the Russian Federal Program Integration and the INTAS Project 97-32174. The financial support of N.K. by the scientific visitor program of the GeoForschungsZentrum Potsdam GFZ is grate-

fully acknowledged. We thank the Potsdam Institute for Climate Impact Research for access to the supercomputer facilities.

References

Bai Qu, Kohlstedt DL (1993) Effects of solubility and incorporation mechanism for hydrogen in olivine. Phys Chem Miner 19: 460–471

Becke AD (1988) Density-functional exchange-energy approximation with correct asymptotic behaviour. Phys Rev (A) 38(6): 3098–3100

Beran A, Putnis A (1983) A model of the OH positions in olivine derived from infrared-spectroscopic investigations. Phys Chem Miner 9: 57–60

Brodholt JP (1997) Ab initio calculations on point defects in forsterite (Mg_2SiO_4) and implications for diffusion and creep. Am Mineral 82: 1049–1053

Brodholt JP, Refson K (2000) An ab initio study of hydrogen in forsterite and a possible mechanism for hydrolytic weakening. J Geophys Res 105 (B8): 18977–18982

Chinnery NJ, Pawley AR, Clark SM (1999) In situ observation of the formation of 10 Å phase from talc + H_2O at mantle pressures and temperatures. Science 286: 940–942

Goedecker S, Teter M, Hutter J (1996) Separable dual-space Gaussian pseudopotentials. Phys Rev (B) 54(3): 1703–1710

Freund F, Oberheuser G (1986) Water dissolved in olivine: a single-crystal infrared study. J Geophys Res 91: 745–761

Heiber M, Ballone P, Parrinello M (1997) Structure and dynamics of protonated Mg2SiO4: an ab-initio molecular dynamics study. Am Mineral 82: 913–922

Hutter J, Ballone P, Bernasconi M, Focher P, Fois E, Goedecker S, Parrinello M, Tuckerman M (1995–2001) CPMD v. 3.4, MPI für Festkörperforschung and IBM Zürich Research Laboratory

Karki BB, Stixrude L, Clark SJ, Warren MC, Ackland GJ, Crain J (1997) Elastic properties of orthorombic MgSiO3 perovskite at lower mantle pressures. Am Mineral 82: 635–638

Khisina NR, Wirth R, Andrut M, Ukhanov AV (2001) Extrinsic and intrinsic mode of hydrogen occurrence in natural olivines; FTIR and TEM investigation. Phys Chem Miner 28: 291–301

Khisina NR, Wirth R (2002) Hydrous olivine $(Mg,Fe)_{2-x}v_x SiO_4H_{2x}$ – a new DHMS phase of variable composition observed as nanometer-size precipitation in mantle olivine. Phys Chem Miner 29(2): 98–11

Kitamura M, Kondoh S, Morimoto N, Miller G, Rossman GR, Putnis A (1987) Planar OH-bearing defects in mantle olivine. Nature 328: 143–145

Kohlstedt DL, Keppler H, Rubie DC (1996) Solubility of water in the α, β, and γ phases of $(Mg,Fe)_2SiO4$. Contrib Mineral Petrol 123: 345–357

Lasaga AC (1981) The atomistic basis of kinetics: defects in minerals. In: Lasaga AC, Kirkpatrick RJ (eds) Reviews in mineralogy, vol 8. Mineralogical Society America, Washington, DC, pp 261–317

Lee CL, Yang W, Parr RG (1988) Development of the Colle-Salventti correlation energy formula into a functional of the electron density. Phys Rev (B) 37: 785–789

Libowitsky E, Beran A (1995) OH defects in forsterite. Phys Chem Miner 22: 387–392

Liu LG (1987) Effects of H_2O on the phase behaviour of the forsterite–enstatite system at high pressures and temperatures and implications for the Earth. Phys Earth Planet Interiors 49: 142–167

Miller GH, Rossman GR, Harlow GE (1987) The natural occurrence of hydroxyl in olivine. Phys Chem Miner 14: 461–472

Monkhorst HJ, Pack D (1975) Special points for Brellouin-zone integration. Phys Rev B (13): 5188–5192

Sprik M, Hutter J, Parrinello M (1996) Ab initio molecular dynamics simulation of liquid water: comparison of three gradient-corrected density functionals. J Chem Phys 105(3): 1142–1152

Wright K, Catlow CRA (1994) A computer simulation study of OH defects in olivine. Phys Chem Miner 20: 515–518

Wunder B, Schreyer W (1997) Antigorite: high-pressure stability in the system MgO–SiO2–H2O (MSH). Lithos 41: 213–227

Young TE, Green HW II, Hoffmeister AM, Walker D (1993) Infrared spectroscopy investigation of hydroxyl in beta-$(Mg,Fe)_2SiO_4$ and coexisting olivine: implications for mantle evolution and dynamics. Phys Chem Miner 19: 409–422